



## NRC Publications Archive Archives des publications du CNRC

### **Particle size measurement in glass powder beds using optical coherence tomography**

Veilleux, Jocelyn; Moreau, Christian; Lévesque, Daniel; Dufour, Marc; Boulos, Maher

This publication could be one of several versions: author's original, accepted manuscript or the publisher's version. / La version de cette publication peut être l'une des suivantes : la version prépublication de l'auteur, la version acceptée du manuscrit ou la version de l'éditeur.

For the publisher's version, please access the DOI link below. / Pour consulter la version de l'éditeur, utilisez le lien DOI ci-dessous.

#### **Publisher's version / Version de l'éditeur:**

<https://doi.org/10.1117/1.2896455>

*Optical Engineering*, 47, 3, pp. 033601-1-033601-9, 2008-03-21

#### **NRC Publications Record / Notice d'Archives des publications de CNRC:**

<https://nrc-publications.canada.ca/eng/view/object/?id=9b004da8-331e-4d66-a933-e2835e697829>;

<https://publications-cnrc.canada.ca/fra/voir/objet/?id=9b004da8-331e-4d66-a933-e2835e697829>

Access and use of this website and the material on it are subject to the Terms and Conditions set forth at

<https://nrc-publications.canada.ca/eng/copyright>

READ THESE TERMS AND CONDITIONS CAREFULLY BEFORE USING THIS WEBSITE.

L'accès à ce site Web et l'utilisation de son contenu sont assujettis aux conditions présentées dans le site

<https://publications-cnrc.canada.ca/fra/droits>

LISEZ CES CONDITIONS ATTENTIVEMENT AVANT D'UTILISER CE SITE WEB.

**Questions?** Contact the NRC Publications Archive team at

PublicationsArchive-ArchivesPublications@nrc-cnrc.gc.ca. If you wish to email the authors directly, please see the first page of the publication for their contact information.

**Vous avez des questions?** Nous pouvons vous aider. Pour communiquer directement avec un auteur, consultez la première page de la revue dans laquelle son article a été publié afin de trouver ses coordonnées. Si vous n'arrivez pas à les repérer, communiquez avec nous à PublicationsArchive-ArchivesPublications@nrc-cnrc.gc.ca.



# Particle size measurement in glass powder beds using optical coherence tomography

## Jocelyn Veilleux

Université de Sherbrooke  
Department of Chemical Engineering  
2500 de l'Université Blvd.  
Sherbrooke (Québec), J1K 2R1, Canada

## Christian Moreau

### Daniel Lévesque

### Marc Dufour, MEMBER SPIE

National Research Council Canada  
Industrial Materials Institute  
75 de Mortagne Blvd.  
Boucherville (Québec), J4B 6Y4, Canada  
E-mail: christian.moreau@nrc-nrc.gc.ca

## Maher Boulos

Université de Sherbrooke  
Department of Chemical Engineering  
2500 de l'Université Blvd.  
Sherbrooke (Québec), J1K 2R1, Canada

**Abstract.** Optical coherence tomography was used to collect cross-sectional images of glass powder beds consisting of microspheres with diameters ranging from 8 to 175  $\mu\text{m}$ . Images were formed by a collection of individual interferogram envelopes that give the backscattered light amplitude as a function of the optical path in the glass powder bed. The diameter distribution, for microspheres located near the surface of the beds, is obtained by appropriate peak distance measurements on threshold-selected envelopes after having performed the surface profilometry. The measured distributions are in good agreement with those obtained by laser diffraction. When considering the whole powder volume, the evaluation of the mean light penetration depth inside the powder beds proves to be a useful approach to evaluate the mean particle diameter, although no information is obtained on the actual particle size distribution in this case. Two simplified models are introduced to understand the linear relationship observed between the penetration depth and the mean particle size. © 2008 Society of Photo-Optical Instrumentation Engineers. [DOI: 10.1117/1.2896455]

Subject terms: particle sizing; size distribution; optical coherence tomography; glass powders.

Paper 070544R received Jun. 26, 2007; revised manuscript received Nov. 1, 2007; accepted for publication Nov. 8, 2007; published online Mar. 21, 2008.

## 1 Introduction

Particle size measurements are nowadays involved in a variety of industrial processes, such as the manufacture of polymer fillers, of ceramic or metallic powders, and of pharmaceutical products. As well, they have been introduced in biological applications to retrieve the size distributions of cell nuclei and mitochondria, which can be related to the detection of preinvasive cancer cells.<sup>1</sup> In pollution control applications, they are commonly used to monitor aerosols,<sup>2</sup> fumes and exhaust gases,<sup>3</sup> and water.<sup>4</sup> Consequently, a large number of particle sizing techniques have been investigated over the past years, but none has emerged as a universal technique. In fact, to the diversity of applications corresponds a multiplicity of methods, each having its own advantages and drawbacks.<sup>5</sup> To select the appropriate method for a specific application, one has to consider the particle properties to be measured (size, speed, concentration, refractive index, etc.), the environmental constraints (accessibility, temperature, etc.), and the measurement purpose (fine distribution measurement or coarse product control).<sup>6</sup> These considerations will eventually dictate whether to choose sieving, an electrical low-pressure impactor, centrifugation, micrograph and image analysis, an optical technique (holography, laser dual Doppler anemometry, laser diffraction, light scattering spectroscopy, multiwavelength extinction, etc.), or any other method available.

However, optical techniques are usually the most suitable for on-line investigation of particles in industrial

applications,<sup>7,8</sup> since they are generally noninvasive and can be adapted to precisely measure a wide range of particle size, speed, and concentration. Moreover, sensitive hardware components can be remotely located from the in-process sample volume of the particles, the signal being effectively carried through optical fibers. The latter characteristic constitutes an important advantage of low-coherence interferometry (LCI) over traditional diffraction-based optical particle sizers. In fact, diffraction-based particle sizers rely on the measurement of the angular distribution of the light scattered at low angles in the forward direction by the sample.<sup>9</sup> Therefore, it requires a nearby sensor array (or a moving sensor) to detect diffracted light. In a LCI system, both the sample beam and the backscattered signal from the sample are collected through the same optics, reducing the invasiveness of the measuring apparatus. Moreover, LCI can be combined with light scattering spectroscopy to determine particle size and refractive index by measuring variations in scattering distributions with angle<sup>10,11</sup> or wavelength.<sup>12</sup> Such systems couple a broadband light source into a Michelson interferometer to provide depth resolution, as in optical coherence tomography (OCT), and include an imaging system that permits the variation of the reference field angle in the detector plane. Probing results were obtained on polystyrene microsphere suspensions<sup>11</sup> (with mean diameter of 10  $\mu\text{m}$  or less), and the size determination requires a comparison of measured data with the theoretical predictions of Mie theory. Multiple scattering also proves to have significant effects on the accuracy of results as the penetration depth is increased.<sup>11,13,14</sup>

In the present work, we apply LCI in an OCT system to measure the size distribution of dry glass powders with

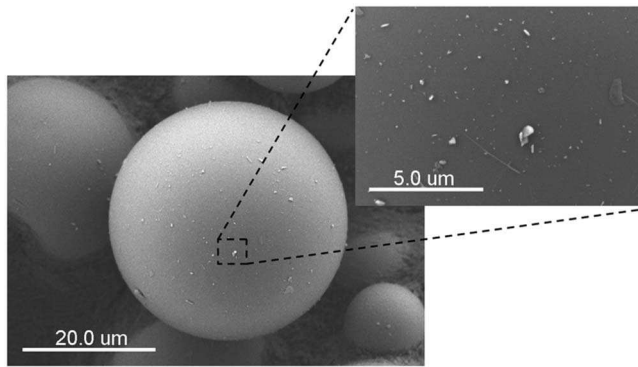


**Fig. 1** SEM micrograph of powder 2, showing its spherical morphology and its surface finish. Small surface roughness appears as white asperities.

mean particle diameter ranging from 8 to 175  $\mu\text{m}$ . One important aspect is that the proposed technique does not use Mie theory to retrieve the scatterer size. Measurements are carried out by inspecting the packed particle beds from the top surface. It is noticed that the lower diameter limit is fixed by the OCT system axial resolution, which depends on the light source coherence length. Microsphere size determination is directly performed on cross-sectional images by first considering the microsphere layers located at the surface of the powder beds. The resulting distributions are in good agreement with those obtained by laser diffraction. In another approach, we investigate the relationship between the mean light penetration depth and the mean particle size in the powder beds. We show that, even in the presence of multiple scattering, the light penetration depth is linearly related to the microsphere diameter. Such a relation is consistent with results obtained by modeling light attenuation in two simplified cases: (i) added contributions of single spherical particles irradiated by a plane wave (Mie theory) and (ii) a stack of glass plates irradiated by a collimated beam.

## 2 Method and Apparatus

Glass powders of five different size distributions were obtained by sieving glass beads used for shot penning. Particle shape, surface finish, and particle size distribution were characterized by scanning electron microscopy (Hitachi S-4700) and by laser diffraction (Beckman Coulter LS 13 320). Figure 1 illustrates the microsphere surface, whereas the size distributions of the five powders investigated in this study are shown in Fig. 6. The glass powders are numbered sequentially from 1 to 5 in order of increasing diameter; their cumulative distribution intervals [10% smaller; 90% smaller] are given by [8;22], [17; 42], [27; 52], [50; 96], and [104; 144]  $\mu\text{m}$ , respectively.

The glass powders were poured into small cups to form dense particle beds and were then imaged using a fiber-based (single-mode SMF-28) OCT system, as shown in Fig. 2. The light emitted by a Covega superluminescent diode (SLD), with a center wavelength  $\lambda$  of 1320 nm and a bandwidth  $\Delta\lambda$  of 70 nm, is divided at a beamsplitter (BS) into two optical paths that are respectively oriented towards the reference mirror and the sample powder. The maximum emitted power is 17 mW, of which only 10% is coupled

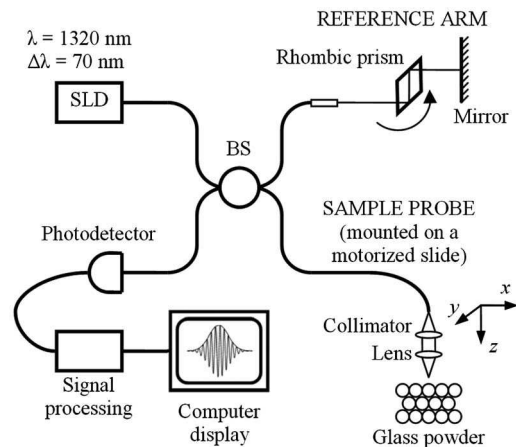


**Fig. 2** Schematic representation of the OCT system. SLD and BS stand for superluminescent diode and beamsplitter, respectively.

into the interferometer, to avoid saturation of the photodetector (Thorlabs FGA-04). When the light returns, if the optical path length mismatch between the reference and sample arms is shorter than the light coherence length, the sample backscattered field and the reference field will combine to produce an interference signal (called an interferogram), which is collected by the photodetector, amplified, and digitally processed (filtered and demodulated). Data acquisition is performed by a two-channel, 14-bit analog-to-digital converter running at 4 Msample/s. By recording this interference signal as the reference mirror is synchronously translated, the axial profile of the sample backscattering properties can be obtained.

The axial resolution of the OCT system depends on the coherence length of the light source, and a high resolution can be achieved independently of the sample arm optics. For a Gaussian source, it can be shown<sup>15</sup> that the axial resolution  $\Delta z$  of the OCT system is inversely proportional to the power spectrum bandwidth, that is,  $\Delta z = 2 \ln 2 (\lambda^2 / \Delta\lambda) / \pi$ . The system used in the present experiment has an axial resolution (in air) of 11  $\mu\text{m}$  and a sample probe transverse resolution of about 12  $\mu\text{m}$  (a 2-mm-wide collimated beam focused by a 14.5-mm-focal-length lens). The collecting numerical aperture of the system is  $\text{NA} = 0.07$ . The focal spot is located approximately at the powder surface. For each powder, 16 cross-sectional images (or *B scans*) were collected, a single *B scan* being formed by 2000 contiguous interferograms (or *A scans*). Scanning is performed by moving the probe over the surface using a motorized slide driven by a stepper motor. The step size between two successive interferograms was adjusted to 1  $\mu\text{m}$ , while the probing depth step size (on the optical axis) was set to  $\lambda/8 = 0.165 \mu\text{m}$  when collecting the interferogram. However, during the demodulation process, each envelope was resampled at 1 point/ $\mu\text{m}$ . The optical delay line is made of a rotating rhombic prism mounted on a galvanometer; it has a scanning rate of 148 Hz and a maximal probed depth of 4 mm (details of the optical delay line are given elsewhere<sup>16</sup>). The separation between two consecutive cross-sectional images was held at 50  $\mu\text{m}$ .

### 3 Results and Discussion

#### 3.1 Cross-Sectional Images

Cross-sectional imaging of glass powder beds was performed, and images are shown in Fig. 3. The grayscale is divided into 256 levels to plot the matrix  $B$  of the normalized logarithmic amplitude given by

$$B = \frac{\log_{10}A}{\max[\log_{10}A]}, \quad (1)$$

where  $A$  stands for the signal amplitude as collected by the OCT system and  $\max[\ ]$  is the maximum value of the expression inside the brackets (the maximal value being taken over the whole cross-sectional image).

Three particularities can be noted when analyzing the cross-sectional images shown in Fig. 3. Firstly, when the microsphere diameter increases, it becomes easier to distinguish individual microspheres at the surface of the powder bed, since local air-glass and glass-air interfaces generate a clearly resolved structure. However, for larger penetration depth, no structural peak can be identified in the background of multiply scattered signal and noise. Secondly, the observed light penetration depth seems larger for larger particle diameters. This observation can be explained by the reduction of the number of scattering sites per unit volume when the microsphere diameter increases. Thirdly, almost the whole top hemisphere of particles at the bed surface can be observed in the cross-sectional image of powder 5. This may appear surprising in that a perfectly focused light beam on the apex of a single and smooth microsphere should prevent such a result. The observation is attributed to the surface roughness of the particles, which generates diffuse reflections (the size of asperities may be as large as the wavelength used, as shown in Fig. 1). Moreover, the finite depth of field of the optical system may contribute to the observation discussed here. Indeed, preliminary ray-tracing simulations on a perfectly smooth microsphere suggest that the relative light intensity coupled into the fiber decays in a slower manner as the probe moves away from the microsphere apex, provided the apex is off focus.

The last observation is not discussed further here, whereas the former two observations (individual microspheres distinguishable near the surface and an apparent increase in penetration depth with particle size) are used to identify two corresponding approaches to retrieve the microsphere diameter: a processing method for the first particle layers (from which the particle size distribution is obtained) and another method based on the calculation of the light penetration depth (from which the mean particle size is obtained).

#### 3.2 Near-Surface Particle Size Distribution

The first investigated approach is based on the hypothesis that maximum signal peaks will be obtained when the sample beam impinges on the apex of a single microsphere surface and exits at the bottom surface (justified by the small  $NA=0.07$ ). Both air-glass and glass-air interfaces crossed along this optical path result in an abrupt refractive index variation that reflects a signal towards the interferom-

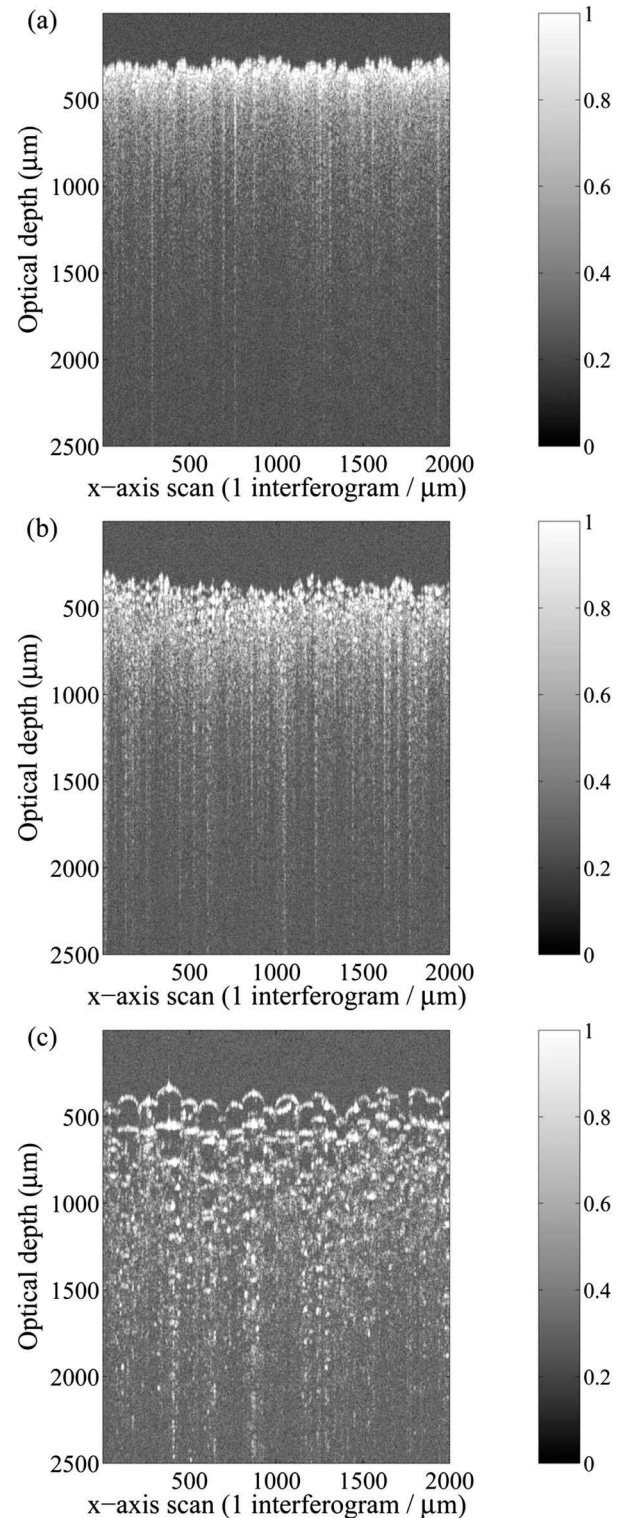


**Fig. 3** Examples of OCT cross-sectional images acquired for (a) powder 1, (b) powder 3, and (c) powder 5. The normalized logarithmic amplitude is represented on a 256-level grayscale.

eter. Therefore, measuring the distance between the corresponding peaks on the interferogram envelope provides an evaluation of the microsphere geometric diameter  $D_{\text{sph}}$  using the expression

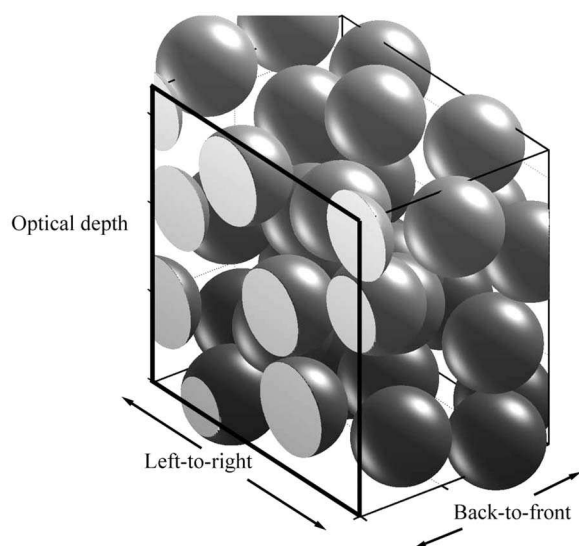


**Fig. 4** Schematic representation of a cross section (shown on front plane) taken on a random close pack of spheres having a uniform diameter.

$$D_{\text{sph}} = \kappa d / n_{\text{glass}}, \quad (2)$$

where  $d$  is the distance between peaks,  $\kappa$  is a correction factor, and  $n_{\text{glass}}$  is the refractive index of the microsphere. The determination of the correction factor  $\kappa$ , which involves the relationship between a spherical particle and a circular trace intersected by a random plane of finite thickness (focal spot width), is not straightforward. Such circular traces are shown for a random close packing of spheres in Fig. 4. Attempts to apply Schwartz-Saltykov method<sup>17</sup> to evaluate the correction factor led to intrinsic difficulties related to the underrepresentation of circular traces having smaller diameters. In fact, light reflections generated away from the apex area of small microspheres (corresponding to powders 1 to 4), which should generate most of the expected smaller circular traces, are hardly collected with OCT. The small numerical aperture and the large focal spot width are the major obstacles. Consequently, calculation of a correction factor based on the Schwartz-Saltykov method does not appear practical at this point, and another method was chosen.

An algorithmic approach was developed to circumvent the correction factor calculation. This is done by selecting interferogram envelopes in cross-sectional images from the local apexes of microspheres. Formally, this envelope selection, applied in a left-to-right manner in cross-sectional images, does not remove the need for a back-to-front plane intersection correction (Fig. 4). However, by applying a proper amplitude threshold algorithm as described below, the additional correction should be made very small, since the reflected light intensity is maximal in two cases: when the center of the focused beam Raleigh range coincides with the apex of a microsphere, and when the beam wave front curvature matches the microsphere curvature. However, on taking into account the sample probe optics used in this experiment, the latter case is seen to be improbable, since it would require microspheres having a diameter larger than 350  $\mu\text{m}$ . Thus, one can safely consider that the

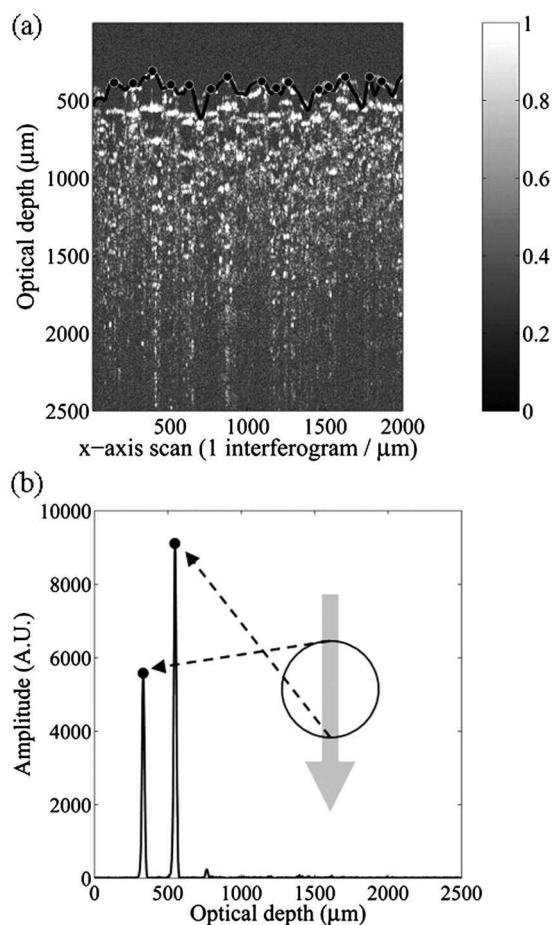


**Fig. 5** (a) Profiliometry of the powder surface (solid black line) and identification of interferogram envelopes corresponding to microsphere apexes (black dots). (b) Linear amplitude of interferogram envelope located at  $x=384 \mu\text{m}$ , showing the relationship between peak positions and microsphere surfaces crossed by the sample beam.

reflected light intensity is maximal when the focused beam Raleigh range coincides with the apex of a microsphere only.

In detail, the approach developed consists in a two-step algorithm applied to each cross-sectional image. The first step performs the profiliometry of the powder bed surface and identifies the interferogram envelopes associated with the local apexes of the microspheres, as shown in Fig. 5(a). With this approach, only one interferogram envelope is selected on each microsphere, avoiding the overrepresentation of larger particles. Then, the second step applies to selected envelopes an amplitude threshold fixed at a certain percentage of the mean amplitude of the most intense peaks in the considered cross-sectional image. In this work, a threshold fixed at 20% of the mean amplitude of the 10 largest peaks was selected. Based on the hypothesis of maximum signal peaks, this second step removes undesired low-amplitude signals and permits the measurement of  $d$ , the distance between peaks, as depicted in Fig. 5(b). Thus, using this algorithm to select appropriate interferogram envelopes almost eliminates the need for a correction factor, and Eq. (2) can be reduced to  $D_{\text{sph}} = d / n_{\text{glass}}$ . From a mea-

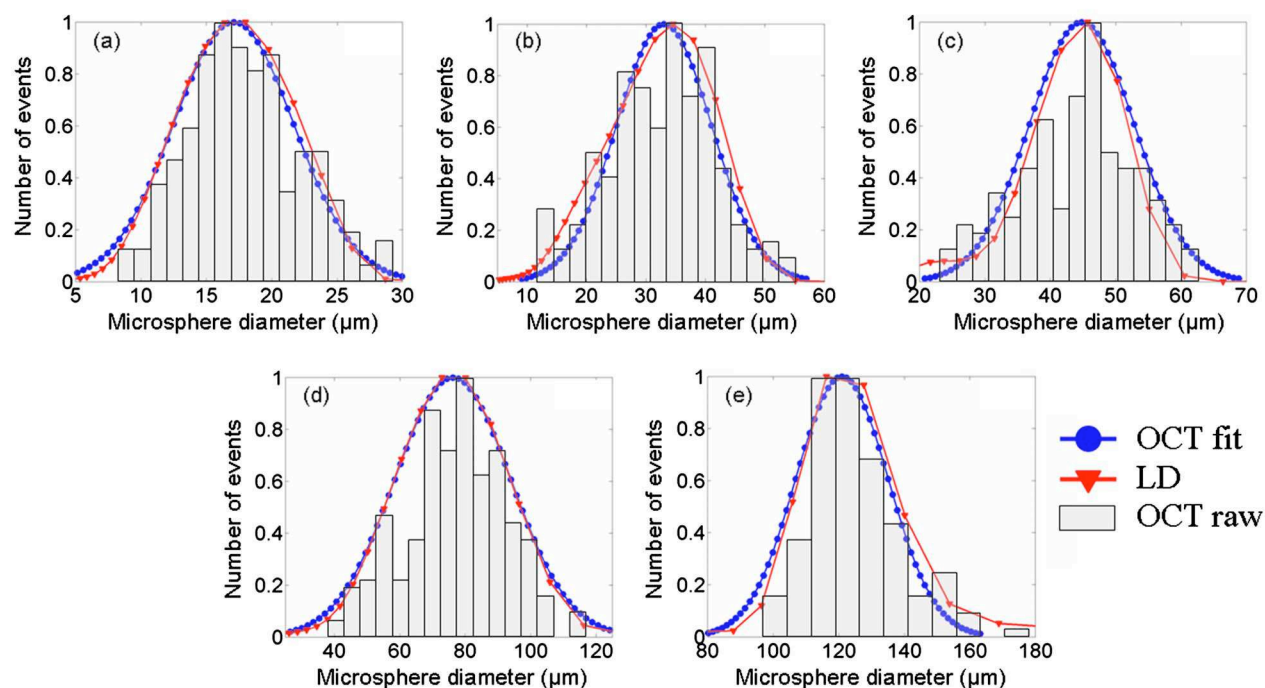


**Fig. 6** Comparison of microsphere size distributions as obtained by optical coherence tomography (OCT) and laser diffraction (LD): (a) to (e) for powders 1 to 5, respectively.

sured  $n_{\text{glass}} = 1.5 \pm 0.1$ , obtained with OCT on a single large microsphere by comparing the geometrical and optical diameters (denoted  $D_{\text{sph}}^{\text{geom}}$  and  $D_{\text{sph}}^{\text{opt}}$ , respectively, with  $n_{\text{glass}} = D_{\text{sph}}^{\text{opt}}/D_{\text{sph}}^{\text{geom}}$ ), the microsphere diameter for all selected envelopes on all cross-sectional images collected can be calculated.

The microsphere diameter data are then used to plot the size distributions of the five powders studied, as shown in Fig. 6. The analysis just described is valid as long as the two analyzed reflections come from the top and bottom surfaces of the same microsphere. If this is not the case, abnormally small or large diameter values can be obtained. For example, an abnormally small diameter value could be due to the presence of noise on a signal generated at a single air-glass interface. Indeed, the algorithm could falsely identify two distinct peaks close to each other, leading to an artificially small diameter value. On the opposite side, if the amplitude of the peak associated with the second interface of a microsphere is smaller than the applied threshold, and if a subsequent peak exceeds this threshold, then the diameter measurement will be biased upwards. In the results presented in Fig. 6, measurements corresponding to 2.5% smaller and larger diameters of the distributions are removed to avoid biasing the results due to those false detections. The resulting OCT size distributions can be fitted with a normal distribution, normalized, and compared with the distributions obtained by laser diffraction, as shown in Fig. 6. The measured distributions are in good agreement with those obtained by laser diffraction. A comparison of the mean values and standard deviations of the two series of measurements is shown in Table 1.

One might expect a shift towards larger diameters of the OCT distribution of powder 1 [Fig. 6(a)], since the optical

axial resolution is limited to  $11 \mu\text{m}$ . However, less than 10% of the microspheres have a geometrical diameter smaller than  $11/1.5 = 7.3 \mu\text{m}$ , and that explains why the expected shift is not observed. Also, notice in Fig. 6(c) the significant left shoulder on the distribution of powder 3 obtained by laser diffraction. Diameters obtained with OCT indeed present this shoulder, but the Gaussian fit in this case results in a slight left shift of the mean and in a larger standard deviation. Overall, the agreement between the two techniques is excellent, and it validates the application of the proposed approach to determining the size distribution of particles located near the surface of the powder beds. One should not expect any difficulty in retrieving the diameter of even larger microspheres (diameter  $> 175 \mu\text{m}$ ) with this technique.

**Table 1** Mean values ( $\mu$ ) and standard deviations ( $\sigma$ ) of the five studied powders as obtained by laser diffraction and OCT.

Powder	Laser diffraction		OCT	
	$\mu$ ( $\mu\text{m}$ )	$\sigma$ ( $\mu\text{m}$ )	$\mu$ ( $\mu\text{m}$ )	$\sigma$ ( $\mu\text{m}$ )
1	15	6	17	5
2	30	9	33	8
3	41	10	45	12
4	73	19	67	18
5	123	17	121	14

### 3.3 Mean Particle Size and Light Penetration Depth

#### 3.3.1 Light penetration depth measurement

The second approach to retrieve diameter-related information from OCT cross-sectional images relies on the apparent relationship between the light penetration depth and the particle diameter, as observed in Fig. 3. An exact description of the propagation of a focused beam inside a highly scattering medium represents a very complex problem.<sup>13,14,18,19</sup> Because such an exact description goes beyond the objectives of the present study, the following development rather aims at establishing a correlation between an OCT signal characteristic (effective light penetration depth) and the mean particle size.

The mean or effective penetration depth  $\delta_{\text{eff}}$  is defined as

$$\delta_{\text{eff}} = \frac{\sum_{i=0}^N z_i A_i}{\sum_{i=0}^N A_i}, \quad (3)$$

where  $z_i$  is the optical depth of the  $i$ 'th point on an interferogram envelope (with  $z_i = \Delta i$ ,  $\Delta$  being the acquisition step size),  $A_i$  is the signal amplitude collected at this depth, and  $N$  is the number of points per interferogram envelope. Equation (3) is used to calculate the penetration  $\delta_{\text{eff}}$  for each interferogram envelope  $j=1, 2, \dots, 2000$  forming the cross-sectional image (not only those corresponding to microsphere apexes), and an average value is calculated.

Theoretically, it can be easily shown that, for an exponentially decaying signal amplitude  $A = A_0 \exp(-z/\delta)$  describing a single-scattering problem,  $\delta_{\text{eff}}$  corresponds exactly to the physical light penetration depth  $\delta$  for a window of sufficiently large optical depth. The mean-penetration-depth calculation proves to be more robust and less prone to interferogram amplitude variations than the usual slope measurement on the logarithmic amplitude plot of  $\ln A = \ln A_0 - z/\delta$ . In particular, the slope measurement is influenced by the significant signal amplitude associated with the first microsphere surface (almost a specular reflection) and by the identification of the optical depth where multiple scattering begins. Thus, a shallower or steeper slope than envisaged might result. It is worth mentioning that the calculation of  $\delta_{\text{eff}}$  as defined in Eq. (3) stays useful when the effects of multiple scattering appear, even though its precise physical interpretation is more difficult to establish in this case. Indeed, the penetration depth obtained with the calculation of  $\delta_{\text{eff}}$  reflects with more accuracy what is truly observed on a B scan (see Fig. 3) than what would be calculated from the slope of the logarithmic amplitude plot of  $\ln A = \ln A_0 - z/\delta$ . Still, a Monte Carlo simulation such as the one conducted by Karamata et al.<sup>19</sup> may help provide a physical interpretation for  $\delta_{\text{eff}}$ .

#### 3.3.2 Results and discussion

Figure 7 illustrates the observed relationship between the penetration depth  $\delta_{\text{eff}}$  of cross-sectional images and the corresponding mean microsphere diameter of the powders. The error bars correspond to the standard deviation of the calculated penetration for the 16 cross-sectional images. As shown in Fig. 7, a linear relationship is found between  $\delta_{\text{eff}}$  and the microsphere diameter. It is interesting to compare the mean penetration depths observed in this study with

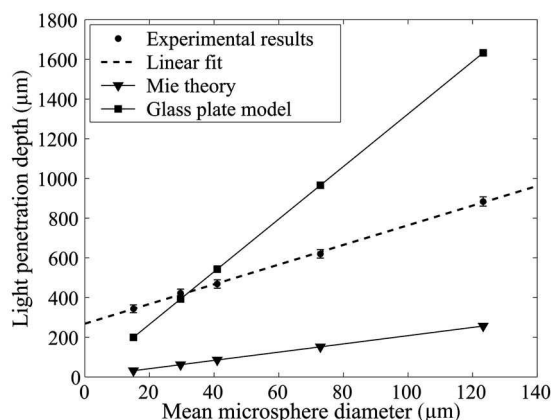


**Fig. 7** Comparison of measured mean penetration depth  $\delta_{\text{eff}}$  with results predicted from the Mie theory and the glass plate model for different microsphere diameters.

theoretical predictions of models that can approximate, as limiting cases, the light scattering in the powder beds. Clearly, these predictions are not exact, but they bring out interesting comparison points to stimulate further research in this field. Figure 7 shows the comparison of observed penetration depths with those based on (i) Mie scattering theory for spheres and (ii) normal incidence of a parallel beam on a stack of glass plates. The illumination conditions in these cases are schematically represented in Fig. 8 and compared with the real situation.

The penetration depth  $\delta_{\text{eff}}$  is much larger than the one theoretically predicted from the Mie theory (see Sec. 5). Strictly speaking, Mie theory does not apply for randomly close-packed powders. Indeed, the large volume fraction of particles, the finite dimension of the light beam, and multiple scattering all limit the validity of a scattering model based on Mie theory. In fact, according to Yadlowsky et al.,<sup>13</sup> multiple scattering significantly reduces the light amplitude decrease below the single-scattering prediction, as observed in the present study. Moreover, the plane wave

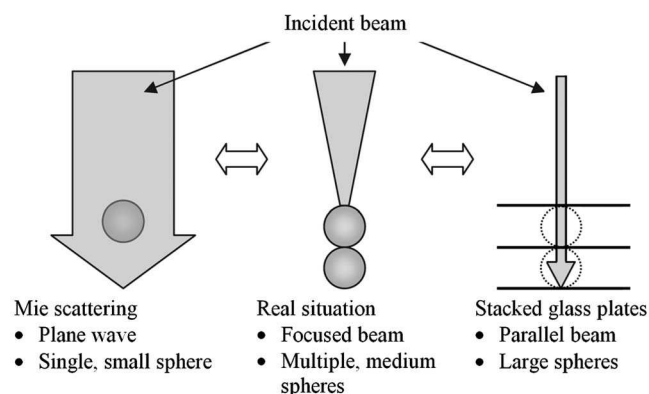


**Fig. 8** Schematic representation of illumination conditions. Mie scattering applies for an incident plane wave over a single small sphere. Real conditions have a focused beam with a size comparable to the size of microspheres illuminated. Stacked glass plates correspond to large microspheres irradiated by a small collimated (parallel) beam.

assumption of the Mie scattering theory is not verified when large glass microspheres are irradiated by a small focused light beam.

In the second model, the scattering problem is reformulated as a collimated beam that impinges on a stack of glass plates (each plate having a thickness close to the microsphere diameter) as illustrated in Fig. 8. Assuming that absorption in the glass is negligible and that the plates are slightly separated by a thin air layer, it is possible to model the light amplitude as a function of depth in the stack (see Sec. 6). Again, this model does not strictly apply to glass powders, but it is interesting for the sake of comparison with the experimental results. According to this model, the measured light penetration should reach between 13 and 16 times the microsphere diameter. Figure 7 shows the case where the light penetration depth is taken at 13 diameters. The experimental penetrations in Fig. 7 differ from the glass plate results by a factor up to 2. The differences might be explained as follows: The light penetration depth from the glass plate model is very dependent on the chosen equivalent transmission coefficient (defined in Sec. 6). When dealing with microspheres, the sample beam incidence angle over air-glass interfaces may differ from normal incidence, some of the light rays being reflected in directions where they are not collected. Therefore, the transmission coefficient used in the model is probably overestimated.

As expected, neither the Mie scattering theory nor the glass plate stacking model successfully reproduces light penetration in a glass powder bed. However, they both show a linear dependence of light penetration on particle diameter, as do the experimental results. Further modeling is needed to understand how the mean penetration depth  $\delta_{\text{eff}}$  is physically related to light penetration when multiple scattering occurs. For example, one can alternatively use geometrical optics and/or a Monte Carlo approach (as suggested earlier) to model the incident light beam energy losses as a result of random focusing and defocusing by microspheres. With such modeling, it will be possible to more confidently use the mean penetration depth  $\delta_{\text{eff}}$  to determine the microsphere diameter from OCT cross-sectional images.

#### 4 Conclusion

The results presented in this study show that OCT can be used to characterize the particle size of compact microsphere beds. The studied microsphere diameters ranged from 8 to 175  $\mu\text{m}$ . Two different approaches were developed to determine, respectively, the actual size distribution and the mean diameter of transparent microspheres at the surface of beds.

The diameter distributions obtained from near-surface interpeak distances on amplitude threshold-selected interferogram envelopes were found to be in good agreement with the actual particle size distributions obtained by laser diffraction. Interestingly, the proposed approach does not refer to the Mie scattering theory to retrieve the particle size distribution. However, the technique shows the limitation imposed by the axial resolution when studying a powder that contains microspheres with an optical diameter smaller than the coherence length of the light source used. Another limitation would be the need for *a priori* knowl-

edge or experimental determination of the refractive index of the scatterers to obtain the size distribution.

It was also shown that the light penetration depth within the powder volume depends linearly on the microsphere diameter. The experimental results were compared with two different light scattering models where this linear dependence is also observed. However, further modeling is needed to derive the mean penetration depth under multiple scattering conditions. Provided that one identifies the clear physical relationship between the effective penetration depth and the microstructure, a study of the relative attenuation as a function of depth may prove to be useful for the discrimination of variations in scatterer size and refractive index with depth, as would be observed in a real biological sample.

#### 5 Appendix: Mie Theory Calculation

The Mie-theory-based model starts by considering single scattering. The signal intensity  $I$  at an optical depth  $z$  can then be expressed as

$$I = I_0 \exp(-\mu_{\text{ext}}z), \quad (4)$$

where  $I_0$  is the initial intensity (at  $z=0$ ) and  $\mu_{\text{ext}} = \Pi\sigma + \mu_a$  is the extinction coefficient, with  $\mu_a$  the absorption coefficient,  $\Pi$  the microsphere number density, and  $\sigma$  the scattering cross section of a single microsphere. We mention here that the signal intensity is chosen in Eq. (4) to be consistent with Mie theory, but that OCT is sensitive to the backscattered field amplitude. At a wavelength of 1.32  $\mu\text{m}$ , absorption in glass can be neglected and the extinction coefficient reduces to the scattering coefficient ( $\mu_{\text{ext}} = \mu_s = \Pi\sigma$ ). However, the scattered light is not completely removed from the incident beam, and a significant portion of optical energy continues to propagate as a forward-scattered component. Therefore, an anisotropy factor  $g$  is introduced to give the so-called reduced scattering coefficient  $\mu'_s = (1-g)\mu_s$ ,<sup>20</sup> which is a better representation of the extinction coefficient under the present imaging condition.

From Eq. (4), we can define the light penetration depth  $\delta$  as the optical path  $z$  for which the intensity ratio is  $I/I_0 = 1/e^2$ . It is equivalent to a detected OCT amplitude ratio of  $1/e$ . Therefore, when using the reduced scattering coefficient and the approximation of weak absorption, the light penetration depth is expressed as

$$\delta_{\text{Mie}} = \frac{2}{1-g} \cdot \frac{2}{\Pi\sigma} = \frac{2}{1-g} \left[ f \left( \frac{\sigma}{v} \right) \right]^{-1}, \quad (5)$$

where  $f$  is the volume fraction of particles and  $\sigma/v$  is the volume scattering coefficient (scattering cross section  $\sigma$  per unit particle volume  $v$ ). Both  $g$  and  $\sigma$  can be calculated as functions of microsphere diameter with the Mie scattering theory.<sup>21</sup> Figure 7 illustrates the light penetration depth for  $f=0.64$  (random close-packed powders), as calculated with Eq. (5).

The applicability of this model is limited by the requirement of small scattering contributions to the total attenuation (i.e.,  $\Pi\sigma h \ll 1$ , with  $h$  being the considered slab thickness). The particle concentration has to be small, which is obviously not the case of random close-packed powders, and multiple scattering cannot be neglected. Moreover, the

incident wave (focused beam) does not verify the plane wave assumption, especially for larger microspheres.

## 6 Appendix: Stack Model

To facilitate modeling of stacked glass plates, the two interfaces (1, glass-air, and 2, air-glass, with transmission and reflection coefficients in amplitude for normal incidence given by  $t_1=1.2$ ,  $r_1=0.2$ ,  $t_2=0.8$  and  $r_2=-0.2$ ) at the junction between two plates are replaced by a single equivalent interface. The latter transmits  $t_1t_2=0.96$  of the amplitude and reflects a proportion  $r_1+t_1t_2r_2=0.008$ . To calculate the amplitude at a depth of  $N$  plates, it is necessary to consider the simple reflection generated at the corresponding interface, but also all the combinations of multiple reflections that give the same optical path. Therefore, with  $t_{eq}=0.96$  and  $r_{eq}=0.008$  respectively standing for the transmitted and reflected amplitudes at an equivalent interface, the following expressions give the asymptotic values of light amplitude  $A$  at a depth of  $N$  plates:

$$\text{minimum amplitude limit: } A(N) > t_1t_2 \times t_{eq}^{2(N-1)} r_{eq}, \quad (6)$$

maximum amplitude limit:

$$A(N) < t_1t_2 \times \sum_{i=1}^N T(N,i) t_{eq}^{2(N-i)} r_{eq}^i 2^{i-1}, \quad (7)$$

where the factor  $t_1t_2$  represents light transmission through the top surface of the first glass plate (in and out). In Eq. (7),  $T(N,i)$  corresponds to the triangle of Narayana numbers.<sup>22</sup> According to this model, the light penetration (defined at the location where  $A/A_0=1/e$ ) reaches a depth between 13 and 16 plates.

## Acknowledgments

The financial support by the Natural Sciences and Engineering Research Council of Canada (NSERC), the National Research Council (NRC) of Canada, and the Fonds Québécois de la Recherche sur la Nature et les Technologies (FQRNT) is gratefully acknowledged. Helpful discussions with Guy Lamouche, as well as the technical support provided by Bruno Gauthier, are greatly appreciated.

## References

1. V. Backman, M. B. Wallace, L. T. Perelman, J. T. Arendt, R. Gurjar, M. G. Müller, Q. Zhang, G. Zonios, E. Kline, T. McGillican, S. Shapshay, T. Valdez, K. Badizadegan, J. M. Crawford, M. Fitzmaurice, S. Kabani, H. S. Levin, M. Seiler, R. R. Dasari, I. Itzkan, J. Van Dam, and M. S. Feld, "Detection of preinvasive cancer cells," *Nature (London)* **406**(6791), 35–36 (2000).
2. P. Demokritou, S. J. Lee, S. T. Ferguson, and P. Koutrakis, "A compact multistage (cascade) impactor for the characterization of atmospheric aerosols," *J. Aerosol Sci.* **35**(3), 281–299 (2004).
3. M. M. Maricq and N. Xu, "The effective density and fractal dimension of soot particles from premixed flames and motor vehicle exhaust," *J. Aerosol Sci.* **35**(10), 1251–1274 (2004).
4. D. J. Law, A. J. Bale, and S. E. Jones, "Adaptation of focused beam reflectance measurement to in-situ particle sizing in estuaries and coastal waters," *Mar. Geol.* **140**(1–2), 47–59 (1997).
5. F. M. Etzler and M. S. Sanderson, "Particle size analysis: a comparative study of various methods," *Part. Part. Syst. Charact.* **12**(5), 217–224 (1995).
6. A. Kleitz and D. Boulaud, "Granulométrie des particules en mouvement et des aerosols," in *Techniques de l'Ingénieur*, Dossier R2360, Paris (1995).
7. D. L. Black, M. Q. McQuay, and M. P. Bonin, "Laser-based techniques for particle-size measurement: a review of sizing methods and

their industrial applications," *Prog. Energy Combust. Sci.* **22**(3), 267–306 (1996).

8. I. Gianinoni, E. Golinelli, G. Melzi, S. Musazzi, U. Perini, and F. Trespidi, "Optical particle sizers for on-line applications in industrial plants," *Opt. Lasers Eng.* **39**(2), 141–154 (2003).
9. J. Swithenbank, J. M. Beer, D. S. Taylor, D. Abbot, and G. C. McCreath, "A laser diagnostic technique for the measurement of droplet and particle size distribution," in *Am. Inst. Aeronaut. Astronaut. 14th Aerospace Sciences Mtg.*, AIAA-1976-69 (1976).
10. A. Wax, C. Yang, R. R. Dasari, and M. S. Feld, "Measurement of angular distributions by use of low-coherence interferometry for light-scattering spectroscopy," *Opt. Lett.* **26**(6), 322–324 (2001).
11. A. Wax, C. Yang, V. Backman, M. Kalashnikov, R. R. Dasari, and M. S. Feld, "Determination of particle size by using the angular distribution of backscattered light as measured with low-coherence interferometry," *J. Opt. Soc. Am. A* **19**(4), 737–744 (2002).
12. C. Xu, P. S. Carney, and S. A. Boppert, "Wavelength-dependent scattering in spectroscopic optical coherence tomography," *Opt. Express* **13**(14), 5450–5462 (2005).
13. M. J. Yadlowsky, J. M. Schmitt, and R. F. Booner, "Multiple scattering in optical coherence microscopy," *Appl. Opt.* **34**(25), 5699–5707 (1995).
14. J. M. Schmitt and A. Knüttel, "Model of optical coherence tomography of heterogeneous tissue," *J. Opt. Soc. Am. A* **14**(6), 1231–1242 (1997).
15. M. R. Hee, "Optical coherence tomography: theory," Chap. 2 in *Handbook of Optical Coherence Tomography*, B. E. Bouma and G. J. Tearney, Eds., pp. 41–66, Marcel Dekker, New York (2002).
16. G. Lamouche, M. Dufour, B. Gauthier, V. Bartulovic, M. Hewko, and J. P. Monchalin, "Optical delay line using rotating rhombic prisms," in *Coherence Domain Optical Methods and Optical Coherence Tomography in Biomedicine XI*, J. G. Fujimoto, J. A. Izatt, and V. V. Tuchin, Eds., p. 64292G-6, SPIE, San Jose, CA (2007).
17. E. E. Underwood, "Particle-size distribution," in *Quantitative Microscopy*, R. T. DeHoff and F. N. Rhines, Eds., pp. 149–200, McGraw-Hill, New York (1968).
18. L. Thrane, H. T. Yura, and P. E. Andersen, "Analysis of optical coherence tomography systems based on the extended Huygens-Fresnel principle," *J. Opt. Soc. Am. A* **17**(3), 484–490 (2000).
19. B. Karamata, M. Laubscher, M. Leutenegger, S. Bourquin, and T. Lasser, "Multiple scattering in optical coherence tomography. I. Investigation and modelling," *J. Opt. Soc. Am. A* **22**(7), 1369–1379 (2005).
20. R. Graaff, J. G. Aarnoudse, J. R. Zijp, P. M. A. Slood, F. F. M. de Mul, J. Greve, and M. H. Koelink, "Reduced light-scattering properties for mixtures of spherical particles: a simple approximation derived from Mie calculations," *Appl. Opt.* **31**(10), 1370–1376 (1992).
21. C. F. Bohren and D. R. Huffman, *Absorption and Scattering of Light by Small Particles*, John Wiley & Sons, New York (1983).
22. T. V. Narayana, *Lattice Path Combinatorics with Statistical Applications*, University of Toronto Press, Toronto (1979).



**Jocelyn Veilleux** received his BEng degree in engineering physics in 2004 from École Polytechnique de Montréal (Canada), and his MScA degree in chemical engineering in 2006 from Université de Sherbrooke (Canada), where he conducted a research project in partnership with the Industrial Materials Institute of the National Research Council of Canada. Since September 2006, he has been a PhD candidate in chemical engineering at McGill University, Canada.

His research interests include optical techniques for the visualization and characterization of nanofluids, materials, and plasmas, as well as fundamentals of heat and mass transfer in two-phase systems.



**Christian Moreau** received his master's degree in nuclear physics in 1981 and his PhD in applied physics in 1985 from Université Laval, Québec City, Canada. Currently, he is group leader for surface technologies at the Industrial Materials Institute of the National Research Council of Canada. His main research interests are development and use of optical sensors for thermal spray particles. He is editor-in-chief of the *Journal of Thermal Spray Technology*.



**Daniel Lévesque** received his BS degree in engineering physics in 1983 and his PhD degree in 1990 from École Polytechnique de Montréal, Canada. Since 1990, he has been working at the Industrial Materials Institute of the National Research Council of Canada. At present, he is senior research officer in the Optical Diagnostics of Materials Group of the institute. His research interests include signal processing, wave propagation modeling, and synthetic aperture

imaging in the development of ultrasonic and optical methods for the nondestructive evaluation of materials. He has coauthored twenty refereed journal papers, two invited and fifty contributed papers in conference proceedings, and six U.S. patents in the field.



**Marc L. Dufour** received his BScA degree in 1977 and his MEng degree in 1980 from École Polytechnique de Montréal, Canada. He has worked as a research associate with the National Research Council of Canada since 1980 and has developed several optical sensors for industrial on-line applications: arc welding, steel casting, and wood processing. Since 1999, he has been involved in the development of low-coherence interference (LCI) sensors for industrial in-

spection and catheterized optical coherence tomography (OCT) for biomedical applications.



**Maher Boulos** received his BSc in 1963 from Cairo University, and his MScA in 1968 and PhD in 1972 from the University of Waterloo, Ontario, Canada. Professor Boulos has been in the Department of Chemical Engineering at the Université de Sherbrooke since 1973. His principal research activity is in the area of thermal plasmas, mathematical modeling, and diagnostics of inductively coupled plasma discharges. He has supervised or cosupervised 55 MSc

and PhD students, has published more than 150 papers in refereed scientific literature, has 25 patent applications to his credit, and has coauthored a textbook on thermal plasma fundamentals and applications. He is a member of the Canadian Engineering Academy and was inducted into the ASM TSS Hall of Fame in May 2003. Professor Boulos was the recipient of the J.-Armand Bombardier prize of the ACFAS in September 2003, and the ADRIQ Innovator prize in Nov 2003. He was also the recipient of the Jules Stachiewicz Medal in 1996, offered jointly by the Canadian Society of Chemical Engineering, and the Canadian Society of Mechanical Engineering, for his contributions in the field of heat transfer under plasma conditions.